IOPscience iopscience.iop.org

Home Search Collections Journals About Contact us My IOPscience

Droplet impact on hydrophobic surfaces with hierarchical roughness

This content has been downloaded from IOPscience. Please scroll down to see the full text.

2014 Surf. Topogr.: Metrol. Prop. 2 035002

(http://iopscience.iop.org/2051-672X/2/3/035002)

View the table of contents for this issue, or go to the journal homepage for more

Download details:

IP Address: 130.89.45.233
This content was downloaded on 06/01/2016 at 08:48

Please note that terms and conditions apply.

IOP Publishing Surface Topography: Metrology and Properties
Surf. Topogr.: Metrol. Prop. 2 (2014) 035002 (10pp) doi:10.1088/2051-672X/2/3/035002

Droplet impact on hydrophobic surfaces with hierarchical roughness

M A Raza[1,2], J van Swigchem[1], H P Jansen[1], H J W Zandvliet[1], B Poelsema[1] and E S Kooij[1]

[1] Physics of Interfaces and Nanomaterials, MESA+ Institute for Nanotechnology, University of Twente, PO Box 217, 7500 AE Enschede, The Netherlands
[2] Centre of Excellence in Solid State Physics, University of the Punjab, QAC, Lahore-54590, Pakistan

E-mail: e.s.kooij@utwente.nl

Received 11 May 2014, revised 14 June 2014
Accepted for publication 24 June 2014
Published 15 July 2014

Abstract

We investigate the dynamic properties of microliter droplets impacting with velocities up to 0.4 m s^{-1} on hydrophobic surfaces with hierarchical roughness. The substrates consist of multiple layers of silica microspheres, which are decorated with gold nanoparticles; the superstructures are hydrophobized by chemical modification. The initial impact event is analysed, primarily focusing on the bouncing of the droplets. The number of bounces increases exponentially with substrate hydrophobicity as expressed by the contact angle. The subsequent relaxation regime is analysed in terms of the frequency and damping rate of the droplet oscillations. Both quantities exhibit a substantial decrease for large contact angles. Results are discussed in relation to reports in literature; damping is most likely due to viscous dissipation.

Keywords: superhydrophobicity, hierarchical roughness, dynamic wetting

1. Introduction

The phenomenon of droplet impact on surfaces has been a topic of research interest since the 19th century with the pioneering contribution of Worthington [1]. The impact dynamics can be affected by a variety of parameters, such as impact velocity, liquid density, surface tension, viscosity, droplet size and the roughness and wettability of the solid surface [2]. The dynamic behaviour of droplets impacting on solid surfaces is of fundamental importance due to its industrial applications in various technological areas including inkjet printing, spray painting and coating, spray cooling, pesticide spraying, metal forming, soil erosion due to rain drop impact and turbine wear [3].

In the study of dynamic properties of droplets impacting on solid surfaces, various parameters are of interest, such as the maximum spreading diameter, the 'bouncing' on superhydrophobic surfaces, the rebound height, the contact time, and contact angle variation during and after impact on the surface. Different application areas dictate the relevant parameters to be investigated. For example, in herbicide treatment the maximum spreading diameter is of interest to improve the herbicide efficiency; a key issue is to prevent droplet rebound [4]. On the other hand, to improve the water-cooling of a hot solid, the contact time of the droplet with the surface is an important quantity [5]. In other applications such as anti-contaminating textiles, hydro-protected concrete or windshields, the effect of bouncing off is of relevance [6], since it can be used to assess the stability of the air film trapped by the surface structures, which is essential to prevent wetting by rain drops [7]. The dynamics of droplet impact is considered as a useful tool for characterizing the stability of superhydrophobic surfaces. As such, since the last decade extensive studies have focused on investigating droplet impact on superhydrophobic surfaces, owing to their emerging applications including fog-resistant coatings, impermeable textiles, self-cleaning and anti-coating for lab-on-chip devices [5, 8–17]. Another related study reported the rebound dynamics in droplet–droplet collisions on superhydrophobic surfaces, showing the potential for droplet logic [18].

When a water droplet with a certain velocity impacts on a solid surface, the combined role of potential energy, kinetic energy and liquid surface energy give rise to interesting and complicated phenomena [19]. Typically the droplet adopts different shapes, as frequently observed by high speed imaging. After colliding with the substrate, initial spreading of the droplet gives rise to a deformation of the initially spherical droplet to a pancake-like shape [20, 21]. A marked variation

 © 2014 IOP Publishing Ltd

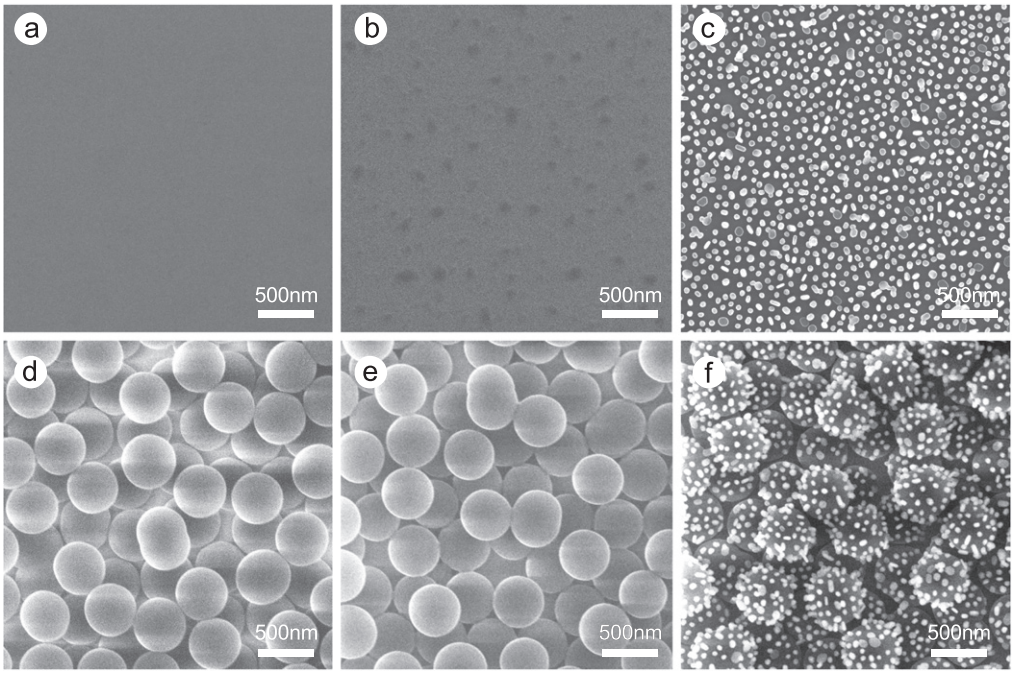

Figure 1. Helium ion microscopy (HIM) images showing the surface morphology of flat, single length scale and hierarchical substrates; the latter consist of 440 nm silica spheres, decorated with 45 nm gold particles. Images (a), (b) show flat oxide-covered silicon surfaces before and after PFOTS treatment, with water contact angles <5° and 110°, respectively. Images (d), (e) show silica sphere arrays before and after derivatization with PFOTS, with contact angles <5° and 148° respectively. Images (c), (f) depict gold nanoparticles on flat silicon and on silica sphere arrays, with contact angles 128° and 162°, respectively. Reprinted from [32], copyright 2012, with permission from Elsevier.

of the contact angle occurs in this stage [22–24]. When the spreading diameter has reached its maximum value, surface tension leads to retraction of the bottom part [25]. Oscillations of the droplet by repeated spreading and retraction of the contact line generally occurs, the spatial extent and duration being dependent on the hydrophobicity of the substrate [26]. On sufficiently hydrophobic surfaces, splashing or rebound [2, 7, 27–31] of the droplet is often seen for a relatively high impact momentum.

Chemical modifications and/or morphologically structuring of substrate surfaces extensively affects the interactions between liquid droplet and solid substrate, resulting in considerable variation of the macroscopic surface wettability. Likewise, the dynamic behaviour of droplets after impact strongly depends on the wetting properties of the surface structure. Recently we have presented a colloidal route to manufacture hierarchical substrates with wetting properties ranging from hydrophobic to sticky or non-sticky superhydrophobic [32]. The surface roughness induced by the combination of silica sphere arrays and gold nanoparticles (see figure 1) in terms of length scale, size and design of surface features was shown to play an important role in dictating the state of the droplets (Wenzel, Cassie–Baxter or mixed) on such substrates [33].

In this work we investigate the dynamics of droplet impact on the aforementioned morphologically nanostructured, hierarchical hydrophobic surfaces. Parameters which are studied as a function of static wetting behaviour include the maximum spreading diameter, the bouncing of droplets, the shape evolution in terms of varying height and contact angle, as well as relaxation behaviour. The results are discussed in terms of available models, while the relaxation behaviour is related to the macroscopic hydrophobicity of the surfaces.

2. Experimental details

2.1. Substrate preparation and characterization

The surfaces with variable roughness were prepared via a bottom-up colloidal route as described in our previous work [32, 33]. The single length scale roughness is achieved by adsorption of either silica spheres of different sizes (850 nm, 440 nm and 130 nm diameter, as determined by scanning electron microscopy) or by deposition of gold nanoparticles of 13 nm, 25 nm and 45 nm. For hierarchical roughness, silica sphere arrays are used as coarser structures, decorated with gold nanoparticles as the finer structures.

Silica sphere arrays were deposited on silicon substrates by means of spin-coating [34, 35]. To enable deposition of gold nanoparticles on flat or hemispherical surfaces, the silica was functionalized with mercaptopropyl-trimethoxysilane; the thiol end groups provide a large affinity for irreversible adsorption of the citrate-stabilized gold nanoparticles [32, 36]. After the colloidal assembly the exposed silica surfaces are functionalized with 1H, 1H, 2H, 2H-perfluorooctyl-triethoxysilane to ensure sufficient stability of the substrates and also to lower the surface energy. Finally, gold nanoparticles are hydrophobized by derivatization with 1-dodecanethiol.

The surface morphology of the nano-/microstructured samples such as that in figure 1 was assessed by scanning helium ion microscope (ORION-Zeiss, USA). For contact angle measurements, the sessile drop method was used on a Dataphysics OCA15+ goniometer under ambient conditions at room temperature (22 °C). Typically, 4–10 μl water droplets were used; contact angle values were determined by the average of at least five independent measurements.

2.2. Droplet impact experiments

In the impact experiments, a droplet of Milli-Q water with a typical volume of 10 μl was created at the tip of a dispensing needle (outer diameter 0.52 mm) using the aforementioned optical contact angle goniometer (DataPhysics OCA15+). The droplet detached from the needle due to gravity and impacts on the substrate at room temperature (22 °C) under ambient conditions. The impact velocity was controlled by varying the distance between the needle and substrate. The dynamic behaviour of the droplet and its impact was recorded using a Photron SA3 high speed camera at a frame rate of 2000 fps; the camera is operated using Photron Fastcan Viewer 3 software. The exact impact velocity was determined from the captured images just before the impact on the substrate.

2.3. Analysis of high speed camera movies

Movies of droplets impacting on the (super)hydrophobic surfaces were analyzed using a home-built 'Matlab' script. For the analysis, the positions of the dispensing needle and the substrate are determined in every frame, including the base line. The drop shape is determined by scanning the regime between needle and substrate row-by-row to find the first and last transition pixel. Relevant physical parameters can be calculated from the extracted drop shape, including (i) the right and left contact angles (using cubic spline algorithm [37]), (ii) height and width, (iii) position of the centre of mass, (iv) the vertical velocity and (v) the number of bounces. The size of the needle is known (0.52 mm diameter), which enables converting the pixel values into real metric values. Typically, a two-second movie at 10 000 fps and 384 × 192 pixels in each frame takes approximately 30 min to complete the analysis (on an Intel Core2Duo CPU, 2.66 GHz).

We also considered using the option to determine the contact angles with the axisymmetric drop shape analysis (ADSA-P) [38], but this is only suitable in static experiments due to the assumption of a 'Laplace pressure' induced droplet profile.

Over 500 movies of droplets on many different hierarchical substrates have been analyzed using the software as described above; transients of all mentioned parameters are stored in a data file. Another Matlab script collects the data from these files for different movies and performs a number of calculations to determine parameters such as the frequency and relaxation rate of the droplet oscillations, diameter of the contact area and the spreading ratio. In figure 2 a typical transient of the height of the centre of mass of a bouncing droplet is depicted. The overall motion of the droplet can be divided into three regimes: (i) the free fall (bold points), (ii) bouncing (dotted line), and (iii) sticky oscillation (solid line). The sticky oscillation can be fitted to a first order damped oscillation [39]. This data is used to classify and compare substrates, as outlined in the following sections.

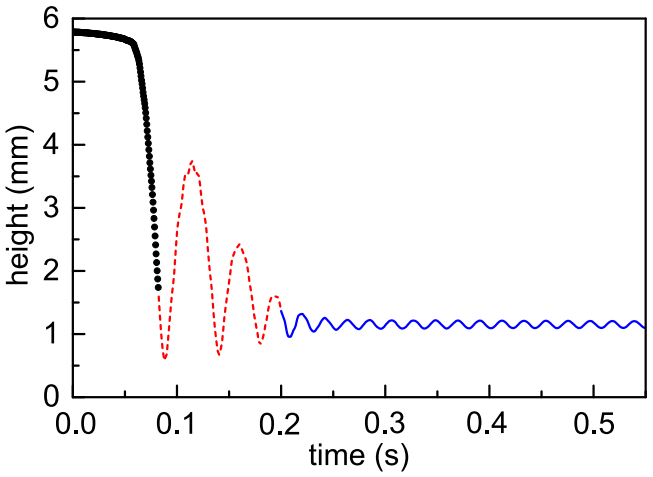

Figure 2. Typical transient of the height of the droplet's centre of mass (10 μl) as extracted from a movie using the analysis software. The bold points indicate the free fall regime, the dotted line represents bouncing (three times), and the solid line the damped oscillation of the droplet.

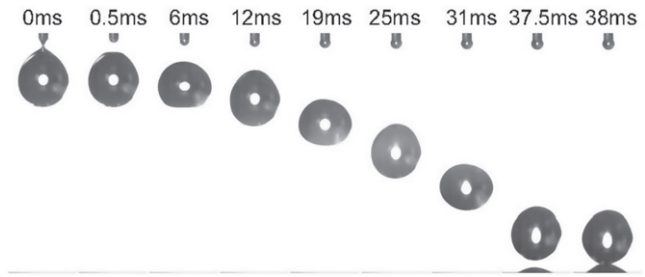

Figure 3. Snapshots of a 10 μl water droplet after detaching from the needle during its free fall under ambient conditions. The droplet oscillates, adopting prolate and oblate shapes. In the last two images (37.5 ms and 38 ms) the reflection of the droplet is visible.

3. Analysis of the falling droplet

A time lapse of a free falling water droplet after detachment from the end of the dispensing needle is shown in figure 3. When the droplet is about to detach (at 0 ms), a 'neck' is formed; the additional surface energy gives rise to enhanced potential energy just before separation. Upon detachment the breaking neck snaps back (at 0.5 ms) and releases this additional energy, therewith producing capillary waves on the surface of the water droplet, as well as on the remaining water in the needle orifice. The droplet deforms continuously [40] from an oblate spheroid (in the image at 12 ms) to a prolate spheroid (image at 19 ms) and vice versa. To evaluate the variation of the outer dimension of the droplet, the horizontal (D_h) and vertical (D_v) diameters were determined as a function of time; the results are shown in figure 4(a).

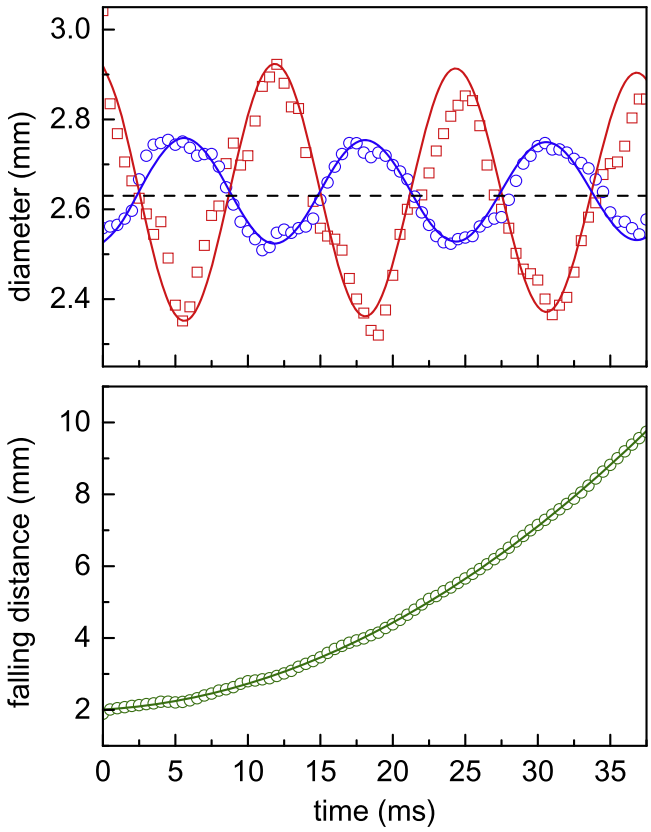

Figure 4. (a) Typical transient of the horizontal (D_h; blue circles) and vertical (D_v; red squares) diameters of a falling droplet; the solid lines represent fit curves as described in the text. (b) The position of the centre of mass of the free falling droplet; the offset of 2.0 mm represents the initial distance h_0 from the needle orifice. The solid line represents a quadratic fit (uniform acceleration), from which an initial velocity $v_0 = 0.023$ m s^{-1} is obtained.

The oscillation behaviour of the droplet during its descent, originating from the aforementioned capillary waves due to detachment, is obvious from the data in figure 4(a). Both the width and the length of the droplet oscillate, of course with the same frequency but 180° out of phase due to the oblate-to-prolate transition. The time-averaged value for the diameter of 2.63 mm is in perfect agreement with the droplet volume of 10 μl. The difference in the amplitudes of the width and the length originates from the geometry of the droplets; the oblate shape has two long (horizontal) axes in perpendicular directions and one short (vertical) axis, while the prolate shape has one long (vertical) axis and two short (horizontal) axes. For small deviation from the spherical shape, a difference of a factor of 2 is expected, which is approximately the case in figure 4(a).

The dynamic behaviour can be analyzed in terms of the pioneering work of Rayleigh and Lamb [41–43]. Assuming small oscillations and neglecting the effect of surrounding gas, the natural frequency of a free droplet of radius R, surface tension γ and liquid density ρ can be evaluated by

$$\omega_n^2 = \frac{\gamma}{\rho R^3} n(n-1)(n+2). \quad (1)$$

The fundamental oscillation mode corresponds to $n = 2$; $n = 1$ represents the rigid spheroid. Owing to the viscosity, the oscillations will be damped in time. For small viscosities, the decrease of the amplitude A with time is given by $A = A_0 \exp(-b_n t)$ with the damping constant defined by

$$b_n = (n-1)(2n+1)\nu/R^2. \quad (2)$$

The latter is a constant, not depending on the restoring force, but only on the size of the droplet and its viscosity. Using parameters for water (surface tension $\gamma = 72.8 \times 10^{-3}$ N m^{-1}, density $\rho = 10^3$ kg m^{-3} and kinematic viscosity $\nu = 10^{-6}$ m^2 s^{-1}), a good fit to our transients is obtained (solid lines in figure 4(a)) using a droplet radius $R = 1.32$ mm, in very good agreement with the actual volume. Moreover, the frequency amounts to 80.1 Hz.

After detachment from the needle, the droplet is in fact a free falling entity; the travelled distance relative to the end of the dispensing needle (figure 4(b)) is quadratic in time. The transient, with an offset of $h_0 = 2.0$ mm due to the initial position below the needle orifice, can be accurately described using uniform accelerated motion under the influence of gravity. From the fit an initial velocity $v_0 = 0.023$ m s^{-1} is obtained, which is ascribed to the aforementioned detachment event. By breaking of the neck, elastic energy is released as kinetic energy. Although straightforward, this analysis enables accurate determination of the impact velocity (the derivative of the curve in figure 4(b)) as a function height from which the droplet is released.

Finally, as mentioned the droplet geometry oscillates between prolate and oblate shapes. In principle this may also have an effect on the relaxation behaviour. We have carefully analyzed our results pertaining to droplets released from different heights; owing to the relatively large scatter of the data, we have not been able to identify any systematic contribution related to the actual droplet shape at the moment of impact.

4. Impact and bouncing regime

When a liquid droplet impinges on a solid surface with a certain impact velocity, the dynamics are governed by a competition of the liquid–solid adhesion force [44, 45] and the inertial behaviour of the droplet [46]. When inertia dominates the dynamics, the droplet bounces off (dotted line in figure 2), which is often referred to as the rebounding or non-wetting regime [47]. If adhesion exceeds the inertial rebound force, a permanent solid–liquid interface is formed and the droplet sticks to the solid surface; this is referred to as the pinning or wetting regime. In figure 5 a series of snapshots are shown for two typical movies in which a 10 μl water droplet impacts on solid surfaces with different morphologies and thus different wetting properties. The results represent (a) the complete rebounding (non-wetting) on a superhydrophobic surface (850 nm silica sphere arrays decorated with gold nanoparticles) and (b) wetting by pinning of the contact line on a hydrophobic substrate (130 nm silica sphere arrays decorated with gold nanoparticles).

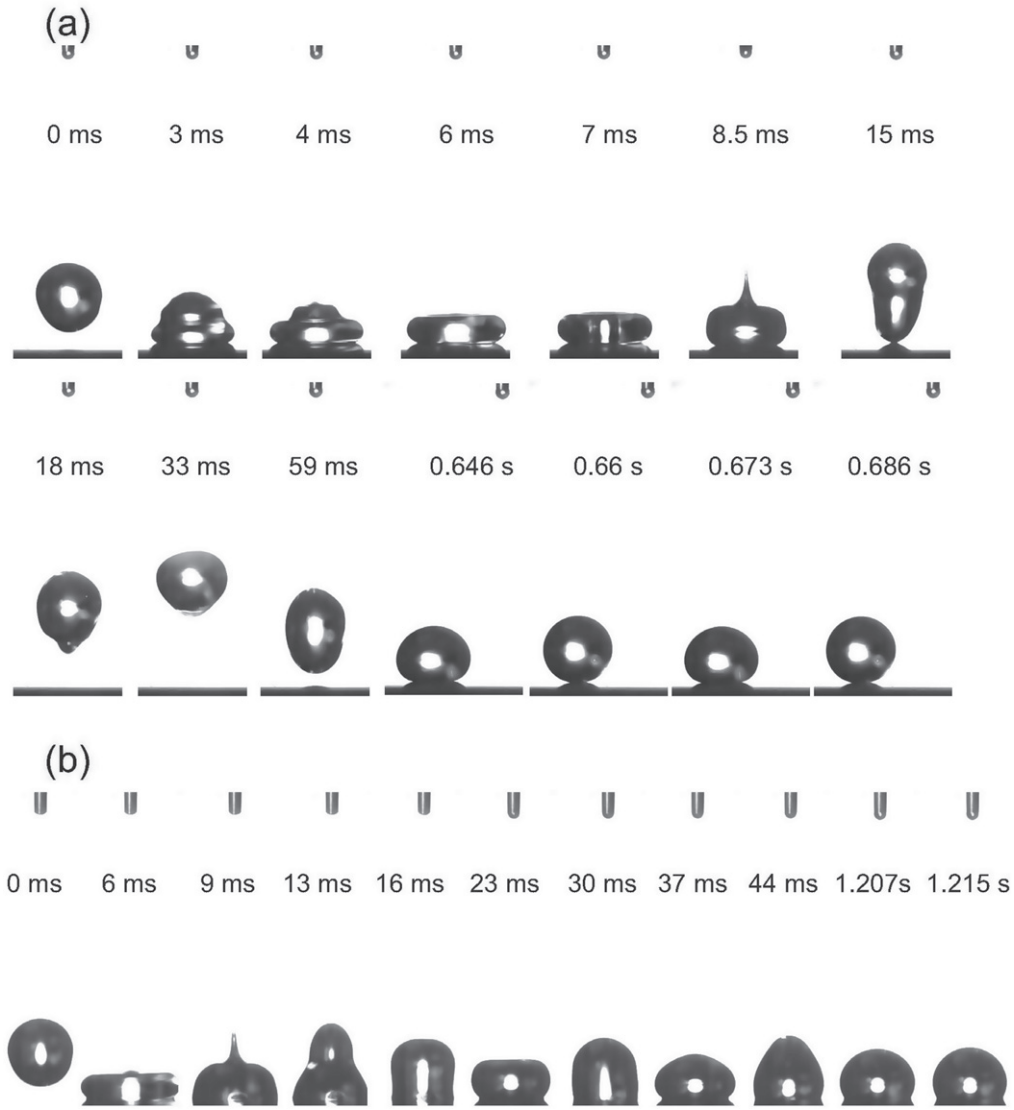

Figure 5. Time lapse of impact events exhibiting (a) jetting, complete rebounding and oscillation on a superhydrophobic surface, and (b) jetting and oscillation on sticky hydrophobic surfaces. The impact velocity in both cases amounts to 0.41 $\pm$ 0.02 m s^{-1}; the liquid volume is 10 μl.

Upon touching the solid substrate, a surface capillary wave is excited and the droplet deforms into a pyramid-like shape as shown by the images at 3 ms and 4 ms in figure 5(a). The droplet spreads to achieve a maximum wetted area (at 6 ms in figure 5(a)) due to inertia; during spreading the kinetic energy is converted into surface energy. The maximum spreading ratio D_{max}/D_0, defined as ratio of the maximum width D_{max} upon impact and the initial diameter $D_0 = 2.63$ mm (see previous section), is often considered as an important parameter [20, 48], which generally depends on the hydrophobicity of the substrate. In our case we find an approximately constant value $D_{max}/D_0 = 1.25$ for the more (super)hydrophobic surfaces. For relatively more wetting surfaces, the smaller advancing contact angles typically lead to higher maximum spreading ratios. We see similar behaviour for our substrates, but for lower contact angle values, the data exhibit considerably larger experimental errors.

Owing to the surface deformation combined with the surface capillary waves, the droplet becomes toroidal, creating a cylinder-like cavity in the centre as can be seen in the image at 7 ms in figure 5(a). Due to air being entrapped when the droplet recoils, a jet is formed [2, 7] as shown in the image at 8.5 ms. The droplet continues to retract as a result of the surface energy and its inertial motion. In the attempt to detach from the substrate, the droplet shape becomes elongated (at 15 ms in figure 5(a)) before taking off. This stretching can be explained by considering the phenomenon of partial or temporary pinning [7], due to wetting and anti-wetting pressures that govern the impact dynamics of the droplet [49]. The wetting pressures are the effective water hammer pressure (P_{WH}) and the dynamic pressure (P_D). The shock wave built up by the compression of the droplet at the contact stage generates P_{WH}, while P_D is due to the kinetic energy of the droplet. The anti-wetting pressure is the capillary pressure caused by the air trapped in

cavities of the rough surface. After a number of bounces the droplet resides on the surface asperities, maintaining its 'fakir' state with air trapped underneath the droplet and thus a large contact angle. However, the remaining kinetic energy after the bouncing regime gives rise to oscillating behaviour before reaching the equilibrium state (last four images in figure 5(a); the actual oscillation lasts longer, typically up to a few seconds). Characteristics such as frequency and decay will be discussed in the next section.

In the case of impact on a sticky hydrophobic surface [32], the droplet is deformed to achieve maximum spreading (at 6 ms in figure 5(b)), followed by recoiling behaviour. Similar jetting as for the non-sticky superhydrophobic behaviour can be observed in this case, as shown in the image at 9 ms. Owing to the strong adhesion between liquid and substrate, the droplet is not able to completely rebound, and does not bounce off. This suggests that the liquid, i.e. water, penetrates into the cavities formed by the surface structure corresponding to the Wenzel state. Again, owing to the kinetic energy, the droplet continues to oscillate like a sticky vibrating sphere as shown in the images after 13 ms in figure 5(b). During the relaxation towards its final equilibrium shape, the dynamics are again governed by a typical frequency and a relaxation rate.

To further investigate the bouncing behaviour of the different substrates, we determined the number of bounces for a range of substrates consisting of silica spheres and the gold nanoparticles constituting the hierarchical roughness. Unfortunately we were not able to identify a clear relation between the (relative) sizes of the micro- and nanoparticles [32, 33] and the wetting properties. The reason for the lack of an obvious trend in these experiments most likely relates to the polydispersity of the particles used in the assembly and also their fairly random distribution on the substrate. Nevertheless, despite a lack of microscopic ordering of the micro- and nanoparticles, the macroscopic wetting properties prove to be reproducible in different spatial locations on the same substrate.

However, despite the absence of such a trend, we still expect the number of bounces to be in some way related to the macroscopic wettability of the substrate, i.e. the equilibrium contact angle of a droplet on such a substrate. On more hydrophobic surfaces, it is easier for the droplet to rebound and bounce off as was observed recently by Crick and Parkin [50]. To verify this, in figure 6 we plot the number of bounces as a function of the final equilibrium contact angle. The latter is obtained by averaging the contact angle over time in the damped oscillation regime (solid line in figure 2). We noted that the equilibrium contact angles of droplets after impacting from a certain height were systematically lower than the static contact angles of droplets gently deposited on the substrates, especially on surfaces with single length scale roughness, either gold nanoparticle layers or silica spheres arrays. We consider this to be due to the fact that for larger impact velocities, the liquid can penetrate further into cavities of the rough surface. As such the overall wetted fraction of the surface increases with impact velocity, approaching more the Wenzel state with relatively lower contact angles [46].

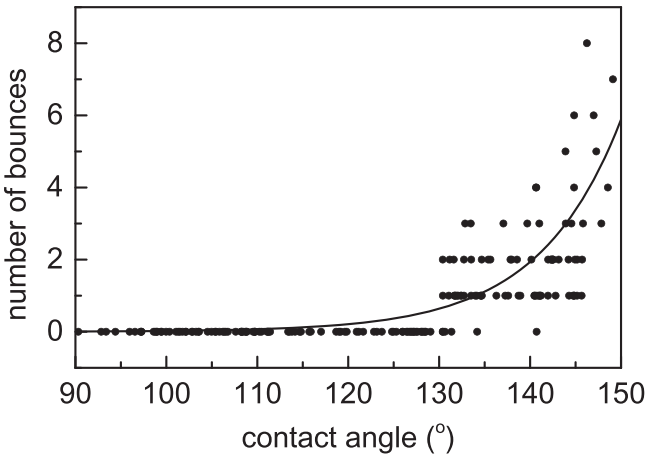

Figure 6. Number of bounces (10 μl droplet) as a function of the equilibrium contact angle. The impact velocity in all cases amounted to 0.41 $\pm$ 0.02 m s^{-1}. The solid line represents an exponential fit, which serves as a guide to the eye.

In agreement with our expectations, the number of bounces increases with the substrate hydrophobicity as characterized by the equilibrium contact angle. Despite the scatter of the data, an obvious trend can be discerned as shown by the exponential fit. The results in figure 6 were obtained by releasing the droplets from the maximum height possible (11.1 mm) within the field of view of the high speed camera. For lower release heights the impact velocity decreases, and therewith also the number of bounces. A similar exponential trend is observed, but at lower values on the vertical axis.

The exponential increase of the number of bounces with increasing (super)hydrophobicity can be rationalized by considering the fact that upon impact the droplet is generally deformed, while wetting the substrate to some extent by advancing the three-phase contact line, followed by a retraction until the droplet detaches. The energy loss corresponding to this process is closely linked to the contact angle hysteresis $\Delta \cos\theta$. In a simple theoretical analysis of bouncing droplets, Wang and co-workers [51] obtained the energy loss W due to the impact event:

$$W = 2A\gamma\Delta \cos\theta, \tag{3}$$

with $A = \frac{1}{4}\pi D_{\max}^2$ the maximum contact area, given by the maximum spreading diameter $D_{\max}$. Recently, we found that the contact angle hysteresis $\Delta \cos\theta$, which is closely linked to the sliding angle, is in good approximation (inverse) linearly dependent on the equilibrium contact angle; a plot of the dynamic contact angles and the sliding angle as a function of static contact angle are plotted in figure 7 [33]. Combined with the fact that the spreading ratio shows little dependence on hydrophobicity, the energy loss thus also decreases linearly with the equilibrium contact angle. After one bounce, the energy loss W gives rise to a lower kinetic energy and as such, the spreading ratio and thus $D_{\max}$ of the second impact will be smaller. The corresponding energy loss also diminishes. This continues until the cumulative energy loss of subsequent bouncing events becomes equal to the initial impact energy. A

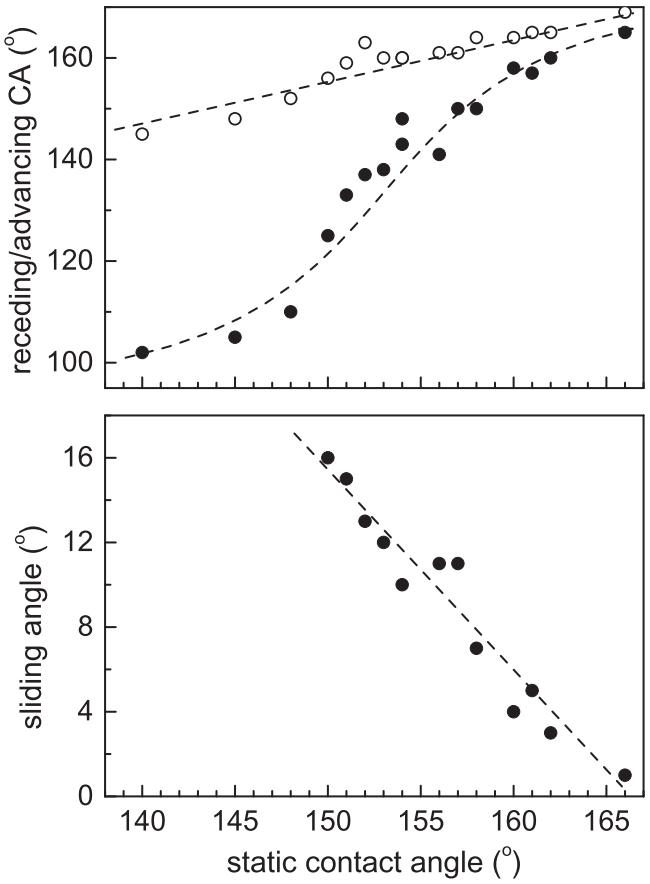

Figure 7. Top: advancing and receding contact angles (open and filled symbols, resp.) as a function of the static contact angle. The dashed lines are a guide to the eye. Bottom: sliding angle as a function of the static contact angle. Results are given for 850 nm silica sphere arrays, decorated with gold nanoparticles with diameters in the range 13–45 nm.

simple analysis indeed confirms an exponential rise of the number of bounces with the equilibrium contact angle, as observed in figure 6.

5. Relaxation regime

In the previous sections we have considered the droplet during its descent after detachment from the needle, and also the impact event accompanied by bouncing of the droplet in relation to the hydrophobicity of the droplet. In this section we study the final stage of the dynamics, characterized by a damped oscillation until the droplet reaches its equilibrium shape. In this damped oscillation regime, the contact line is pinned enabling comparison to existing models [52, 53].

As outlined in the previous section and in previous work [33], we have not been able to identify a clear relation between the length scales of the hierarchical roughness and the observed wetting-related phenomena. However, the hierarchical surface morphologies combined with variation of the wetting properties provide a wide range of equilibrium contact angles. As mentioned, the equilibrium contact angles observed after relaxation of an impacting droplet are

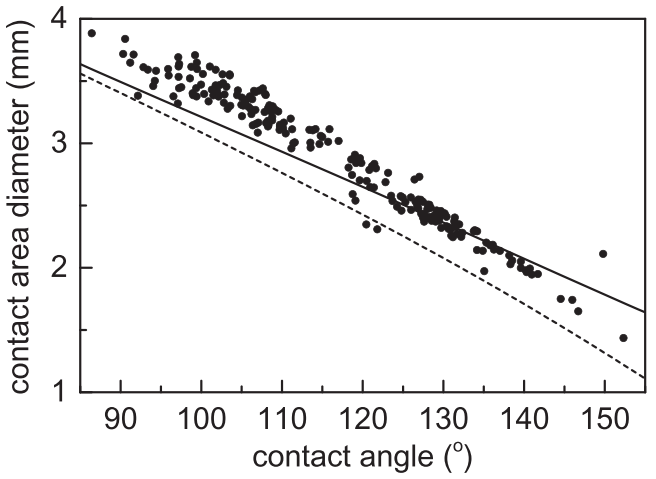

Figure 8. Width of the liquid–solid area as a function of the contact angle after the droplet (10 μl) has relaxed to its equilibrium shape. The dashed line represents a model calculation assuming a spherical cap. The solid line is a calculation based on an analytical model taking into account gravity, as described in the text [55].

systematically smaller than the static contact angles of gently deposited droplets. We ascribe this to a different wetting of the rough surface due to the kinetic energy of the liquid volume coming into contact with the surface. In fact, the contact angles are closer to their receding angles owing to the retraction after the initial spreading.

From the analysis of high speed camera movies, we obtain several parameters as a function of time, including the height of the droplet, the contact angle and the width (or diameter) of the solid–liquid interface. In figure 8 we plot the latter as a function of the contact angle after the droplet (10 μl volume in all cases) has reached an equilibrium situation. Despite the fact that we have considered a variety of surface morphologies (bouncing and non-bouncing) and different impact velocities, the data approximately fall onto a single curve.

In fact, this is to be expected on the basis of the geometry of the droplet. Considering the droplet in equilibrium as a spherical cap, a relation between volume V, radius R and contact angle θ is given by

$$V = \frac{\pi R^3}{3}\left(\cos^3\theta - 3\cos\theta + 2\right), \tag{4}$$

while for the width w of the contact area we use $w = 2R\sin\theta$ [54]. Combining these two expressions, and considering the volume of the droplet ($V = 10\ \mu$l), we obtain the dashed line in figure 8. Although the line reproduces the trend of the experimental data, the contact area seems to be underestimated. It is tempting to ascribed this discrepancy to a difference in the volume of the droplet. However, we verified that the volume of our droplet indeed is $10.0 \pm 0.2\ \mu$l from the geometry of our falling droplet (figure 4). Evaporation of the water during the damped oscillation regime may occur, but for the model to correspond to the data in figure 8, a larger volume is needed.

Another possible cause for the differences may be the fact that in the model a perfectly spherical drop shape is considered. Gravity has been neglected in the aforementioned spherical cap model, while in the actual experiments this gives rise to slightly flattened droplets with a larger contact angle [38, 55, 56]. Rio and Neumann [38] presented a description of the droplet shape, which requires numerically solving a set of differential equations. Two analytical approaches by Shanahan [55] and Fatollahi [56] for droplet shapes under the influence of gravity yield very similar results; they enable a relatively simple quantitative analysis. The solid line in figure 8, obtained using the approach in [55], indeed confirms the assumption that gravity leads to a larger contact area. Although the agreement with the experimental data is slightly improved, there still seems to be a systematic error for which we have no explanation. We also attempted to use smaller droplets, but unfortunately the accuracy of controlling the volume and determining the contact angles decreases substantially for lower volumes.

Similar to the definition of the maximum spreading ratio in the previous section, the equilibrium spreading factor D_{eq}/D_0 is often considered to be relevant, especially for inkjet application purposes [48, 57]. Although we are in a different regime with respect to droplet volume, the spreading factor follows directly from figure 8, by dividing the values by $D_0 = 2.63$ mm. We obtain values decreasing from 1.48 at contact angles near 90° to values as low as 0.57 on superhydrophobic surfaces.

The height of the droplet's centre of mass during the oscillation regime in figure 2 (solid line) can be accurately described using the damped oscillation equation given by

$$h(t) = h_{eq} + Ae^{-\Gamma t}\cos(\omega t + \varphi), \quad (5)$$

where h_{eq} is the equilibrium height, A is the initial amplitude, Γ is the relaxation rate, ω is the angular frequency and φ is a phase factor. Before considering the relaxation rate, we first turn our attention to the frequency.

In figure 9 the resonance frequency for two droplet volumes (10 μl and 5 μl) is shown as a function of the equilibrium contact angle. The results suggest that there is a linear relation between these two quantities. For much smaller droplets, a similar linear relationship was reported by Brown *et al* [48], albeit over a smaller range of hydrophobic contact angles. The frequency in our results decreases from approximately 85 Hz at contact angles near 90° to values around 40 Hz for superhydrophobic surfaces.

On a superhydrophobic surface the droplet adopts an approximately spherical shape. As such we can compare this frequency to that of a freely suspended droplet (result in figure 4). The considerably lower resonance frequency for the sessile droplet can be rationalized by the fact that the centre of mass moves vertically in an oscillatory motion, whereas it does not for the free droplets, such as that in figure 4.

A more quantitative analysis of the resonance frequency can be performed using the model of a spherical cap in contact with a supporting substrate [52, 53, 58, 59]. This model yields values for the oscillation frequency as a function

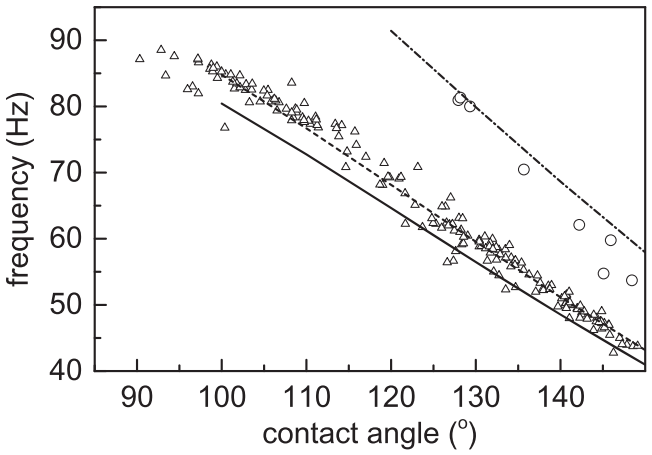

Figure 9. Frequency of the dominant first order resonance during the damped oscillation regime as a function of the equilibrium contact angle. Droplet volumes of 10 μl (triangles) and 5 μl (circles) were considered. The lines represent calculations using the model described in the text [52, 58]. The solid, dashed and dash-dotted lines correspond to 10.0 μl, 9.0 μl and 5.0 μl, respectively.

of surface tension, density, droplet dimension and contact angle. We note that in the work of Strani and Sabetta [52, 53], the contact angle is defined differently. For the regime of contact angles considered here, the frequency is approximately linear in the contact angle. When we insert the appropriate parameters for our droplets of 10.0 ± 0.2 μl, we obtain the solid line in figure 9.

The model appears to underestimate the frequency over the entire range of contact angles, with the largest deviations at smaller angles. The only adjustable parameter is the volume. For a smaller droplet of 9.0 μl, good agreement between calculated and measured data is obtained (dashed line in figure 9). However, the model neglects gravity; we already discussed its possible effect on the contact angles in relation to figure 8. A similar effect may also be observed here, in that the effective equilibrium contact angles are somewhat larger than those for a spherical cap shape with the same volume. The agreement between experiment and calculation for the smaller droplets of 5.0 ± 0.2 μl (circles and dash-dotted line), on which gravity has a smaller effect, confirms this assumption.

Finally, we focus on the damping of the oscillation amplitude with time. For levitated, i.e. free droplets, the damping only depends on the viscosity and the size; the damping is linear in the viscosity and inversely proportional to the radius squared [43, 54]. Here we consider sessile water droplets with a fixed volume (10 μl), where only the hydrophobicity of the substrate with hierarchical roughness is varied. In figure 10 we plot the relaxation rate Γ as a function of the equilibrium contact angle. For this plot we included many experiments with different impact velocities. Only the damped oscillation regime was considered. The fact that the results more or less follow a single curve suggests that the behaviour in the relaxation stage does not depend on whether or not bouncing occurred. This implies that whether the droplet is in the Cassie–Baxter state (at high contact angles)

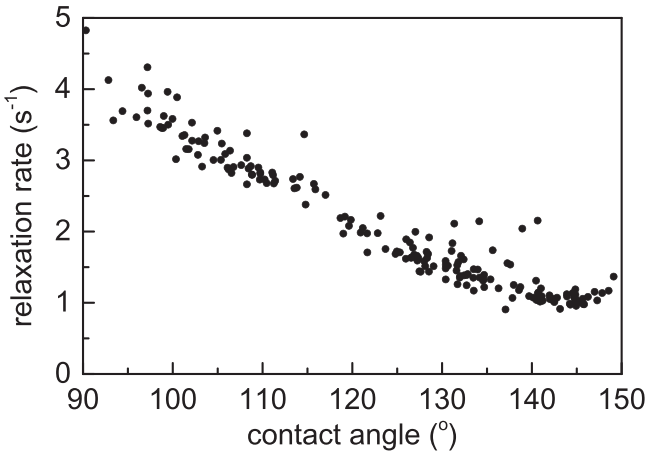

Figure 10. Relaxation rate Γ of the damped oscillation as a function of the equilibrium contact angle for 10 μl droplets on surfaces with varying morphology.

or in the Wenzel or mixed state (at low contact angles where bouncing does not occur) has no effect on the relaxation characteristics.

The variation of the relaxation rate clearly depends on the equilibrium contact angle. From 90° toward 150° the relaxation rate decreases approximately by a factor of 4, implying that damping is considerably reduced for more hydrophobic surfaces. There are a number of possible damping mechanisms that may play a role in sessile droplets related to the presence of a solid boundary and a three-phase contact line, which do not occur in free or levitated droplets [54, 60]. These include bulk viscous dissipation, as well as solid boundary layer effects. It has been suggested that the moving contact line may also give rise to damping [61–64]. However, analysis of our movies shows that in the damped oscillation regime the contact line is pinned, and as such cannot contribute to damping effects.

Bulk viscous dissipation occurs both in free and sessile droplets. In the latter case, however, an additional geometric factor takes into account the contact angle dependence of the damping. For sessile droplets, the presence of a solid boundary, i.e. the substrate, will also influence the damping of capillary waves on the surface of the droplet [60, 65]. The assumption of a no-slip boundary condition at the solid interface means that the fluid velocity must drop from a finite value to zero within a small distance of the solid boundary. This introduces a steep velocity gradient, giving rise to non-negligible energy dissipation in the fluid.

In a recent report, Sharp [54] has provided an overview of possible mechanisms for damping in sessile droplets. On the basis of experiments with droplets of different mass and viscosity, it proved difficult to distinguish between the different mechanisms. Moreover, the treatment of interfacial effects in the work by Sharp is rather basic, and relies on expressions derived for waves on planar liquid surfaces.

Recent numerical simulations [66] were focussed on the frequency and damping of oscillating sessile droplets. Comparing these simulation results to our experimental findings in figure 10 reveals a very similar trend but at different absolute values. On the basis of their work, Olgac and co-workers consider viscous damping to be the most prominent contribution to the damping. More detailed theories for damping at the solid–liquid and liquid–air interfaces must be derived, especially for the relatively large contact angles as considered in this work. Our experimental results may provide an input for future work in this field.

6. Conclusions

We have performed a systematic study of the behaviour of droplets impinging on (super)hydrophobic surfaces with hierarchical roughness, consisting of silica microsphere arrays which are decorated with gold nanoparticles. Immediately after release from the dispensing needle, the droplets exhibit shape deformations between oblate and prolate during their descent toward the surface. These oscillations, which can be analysed in terms of existing models for levitated droplets, do not affect the dynamics during or after impact on the surface. The only parameter which is relevant in this respect is the impact velocity.

Immediately after impact, the non-wetting behaviour of the substrates gives rise to repulsion of the liquid, which leads to multiple bouncing before eventually residing on the surface. The number of bounces was found to depend both on the impact velocity and the hydrophobicity of the substrate; the latter is directly related to the equilibrium contact angle. The data exhibit considerable scatter, but a trend can be discerned where the number of bounces increases exponentially with contact angle. Considering the energy loss due to contact angle hysteresis during the short contact with the substrate, such an exponential trend can be rationalized.

After the impact and bouncing regime, the droplets exhibit damped oscillations. Both the frequency and the relaxation rate were shown to depend strongly on the contact angle. With increasing hydrophobicity, the frequency decreases linearly with contact angle, in line with previous literature reports. The damping rate also exhibits a decline for increasing contact angle, again in agreement with available experimental data. The possible damping mechanisms have been reviewed but the data does not allow a clear identification of the exact mechanism. More work is needed, both experimentally and theoretically, to quantitatively elucidate the results we have presented for hydrophobic substrates with hierarchical roughness over a relatively large range of contact angles.

Acknowledgments

The authors thank Michiel Musterd (TU Delft) for helpful discussions. One of the authors (MA Raza) acknowledges support from the Higher Education Commission of Pakistan.

References

[1] Worthington A M 1876 *Proc. R. Soc.* **25** 261–72
[2] Tsai P, Pacheco S, Pirat C, Lefferts L and Lohse D 2009 *Langmuir* **25** 12293–8
[3] Bolleddula D A, Berchielli A and Aliseda A 2010 *Adv. Colloid Interface Sci.* **159** 144–59
[4] Wang M J, Lin F H, Ong J Y and Lin S Y 2009 *Colloid Surf.* A **339** 224–31
[5] Richard D, Clanet C and Quéré D 2002 *Nature* **417** 811
[6] Callies M and Quéré D 2005 *Soft Matter* **1** 55
[7] Chen L, Xiao Z, Chan P C H, Lee Y K and Li Z 2011 *Appl. Surf. Sci.* **257** 8857
[8] Quéré D 2008 *Annu. Rev. Mater. Res.* **38** 71–99
[9] Shirtcliffe N J, McHale G, Atherton S and Newton M I 2010 *Adv. Colloid Interface Sci.* **161** 124
[10] Richard D and Quéré D 2000 *Europhys. Lett.* **50** 769
[11] Biance A L, Clanet C and Quéré D 2004 *Phys. Rev.* E **69** 016301
[12] Bartolo D, Josserand C and Bonn D 2006 *Phys. Rev. Lett.* **96** 124501
[13] Reyssat M, Pépin A, Marty F, Chen Y and Quéré D 2006 *Europhys. Lett.* **74** 306
[14] Jung Y C and Bhushan B 2008 *Langmuir* **24** 6262
[15] Hyväluoma J and Timonen J 2008 *Europhys. Lett.* **83** 64002
[16] Brunet P, Lapierre F, Thomy V, Coffinier Y and Boukherroub R 2008 *Langmuir* **24** 11203
[17] Rioboo R, Voue M, Vaillant A and Coninck J D 2008 *Langmuir* **24** 14074
[18] Mertaniemi H, Forchheimer R, Ikkala O and Ras R H A 2012 *Adv. Mater.* **24** 5738–43
[19] Yarin A L 2006 *Annu. Rev. Fluid Mech.* **38** 159
[20] Clanet C, Béguin C, Richard D and Quéré D 2004 *J. Fluid Mech.* **517** 199–208
[21] Jansen H P, Sotthewes K, Ganser C, Teichert C, Zandvliet H J W and Kooij E S 2012 *Langmuir* **28** 13137–42
[22] Berim G O and Ruckenstein E 2004 *J. Phys. Chem.* B **108** 19330
[23] Werner S R, Jones J R, Paterson A R H and Pearce D L 2007 *Chem. Eng. Sci.* **62** 2336
[24] Sikalo S, Tropea C and Ganic E N 2005 *J. Colloid Interface Sci.* **286** 661–9
[25] Dodge F T 1988 *J. Colloid Interface Sci.* **121** 154
[26] Dong H, Carr W W, Bucknall D G and Morris J F 2007 *AIChE J.* **53** 2606
[27] Xu L, Zhang W W and Nagel S R 2005 *Phys. Rev. Lett.* **94** 184505
[28] Xu L 2007 *Phys. Rev.* E **75** 056316
[29] Lau K K S, Bico J, Teo K B K, Chhowalla M, Amaratunga G A J, Milne W I, McKinley G H and Gleason K K 2003 *Nano Lett.* **3** 1701
[30] Wang Z, Lopez C, Hirsa A and Koratkar N 2007 *Appl. Phys. Lett.* **91** 023105
[31] Im M, Im H, Lee J H, Yoon J B and Choi Y K 2010 *Soft Matter* **6** 1401
[32] Raza M A, Kooij E S, Zandvliet H J W and Poelsema B 2012 *J. Colloid Interface Sci.* **385** 73–80
[33] Raza M A, Zandvliet H J W, Poelsema B and Kooij E S 2014 in preparation
[34] Wang D and Möhwald H 2004 *Adv. Mater.* **16** 244
[35] Raza M A, Kooij E S, Silfhout A v and Poelsema B 2010 *Langmuir* **26** 12962
[36] Brown K R, Walter D G and Natan M J 2000 *Chem. Mater.* **12** 306
[37] Bortolotti B M, Brugnara M, Della Volpe C and Sibone S 2009 *J. Colloid Interface Sci.* **336** 285–97
[38] del Río O I and Neumann A W 1997 *J. Colloid Interface Sci.* **196** 136–47
[39] van Dam D B and Le Clerc C 2004 *Phys. Fluids* **16** 3403–14
[40] Wang M J, Lin F H, Hung Y L and Lin S Y 2009 *Langmuir* **25** 6772
[41] Rayleigh L 1897 *Proc. R. Soc.* **29** 71
[42] Lamb H 1932 *Hydrodynamics* (New York: Dover)
[43] Archidiacono S and Poulikakos D 2004 *Phys. Rev.* E **70** 011505
[44] Joanny J F and de Gennes P G 1984 *J. Chem. Phys.* **81** 552
[45] Lee S W and Laibinis P E 2000 *J. Am. Chem. Soc.* **122** 5395
[46] Jung Y C and Bhushan B 2009 *Langmuir* **25** 9208
[47] Bormashenko E, Pogreba Y, Whymann G and Erlich M 2007 *Langmuir* **23** 6501
[48] Brown P S, Berson A, Talbot E L, Wood T J, Schofield W C E, Bain C D and Badyal J P S 2011 *Langmuir* **27** 13897
[49] Deng T, Varanasi K K, Hsu M, Bhate N, Keimel C, Stein J and Blohm M 2009 *Appl. Phys. Lett.* **94** 133109
[50] Crick C R and Parkin I P 2011 *Chem. Commun.* **47** 12059
[51] Wang B B, Zhao Y P and Yu T 2011 *J. Adhes. Sci. Technol.* **25** 93–108
[52] Strani M and Sabetta F 1984 *J. Fluid Mech.* **141** 233
[53] Strani M and Sabetta F 1988 *J. Fluid Mech.* **189** 297
[54] Sharp J S 2012 *Soft Matter* **8** 399
[55] Shanahan M E R 1984 *J. Chem. Soc., Faraday Trans.* I **80** 37–45
[56] Fatollahi A H 2012 *Phys. Scr.* **85** 045401
[57] Son Y, Kim C, Yang D H and Ahn D J 2008 *Langmuir* **24** 2900
[58] Smithwick R W and Boulet J A M 1989 *J. Colloid Interface Sci.* **130** 588
[59] Yamakita S, Matsui Y and Shiokawa S 1999 *Japan. J. Appl. Phys.* **38** 3127
[60] Timonen J V I , Latikka M, Ikkala O and Ras R H A 2013 *Nat. Commun.* **4** 2398
[61] Vukasinovic B, Smith M K and Glezer A 1995 *J. Fluid Mech.* **291** 323
[62] Christiansen B, Alstrøm P and Levinsen M T 1995 *J. Fluid Mech.* **291** 323
[63] Miles J 1991 *J. Fluid Mech.* **222** 197
[64] Hocking L M 1987 *J. Fluid Mech.* **179** 253
[65] Milner S T 1991 *J. Fluid Mech.* **225** 81
[66] Olgac U, Izbassarov D and Muradoglu M 2013 *Comput. Fluids* **77** 152–8